表２　脂質クラスによる分子量関連正負イオンの特徴

CE, Wax, TG, DG	$[M+NH_4]^+$	
Cer, GlcCer, PC, SM, & LPC	$[M+H]^+$	$[M+HCOO]^-$
PG, PI, PA, Car, & LBPA	$[M+NH_4]^+$	$[M-H]^-$
PE, PS, & LPE	$[M+H]^+$	$[M-H]^-$

CE, cholesterol ester; TG; triacylglycerol; DG, diacylglycerol; Cer, ceramide; GlcCer, glucosylceramide; LBPA, lysobisphosphtidic acid;

PG, phosphatidylglycerol; Car; cardiolipinPE, phosphatidylethanolamine;

PI, phosphatidylinositol; PS, phosphatidylserine; PC, phosphatidylcholine;

SM, sphingomyelin; LPC, lysophosphatidylcholine;

LPE, lysophosphatidylethanolamine.

図1

A. 代謝の理解に便利な分類

1. 単純脂質 (C,H,Oからなりアセチル CoAから生合成される。複合脂質の構成成分)
   脂肪酸と誘導体、ステロイド(イソプレノイド)

2. 複合脂質 (N,P,Sなども含む)
   a) グリセロ脂質 (グリセロール骨格を持つ)
      グリセロリン脂質
      アシルグリセロール
      グリセロ糖脂質

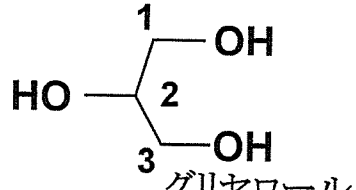

グリセロール

   b) スフィンゴ脂質 (スフィンゴシン骨格を持つ)
      スフィンゴリン脂質
      スフィンゴ糖脂質

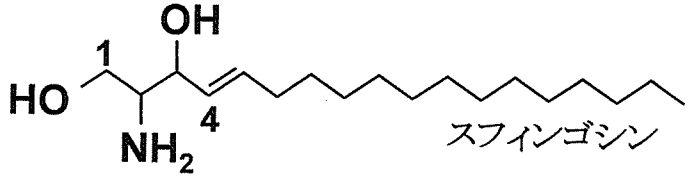

スフィンゴシン

B. データベース用包括的分類[1)]

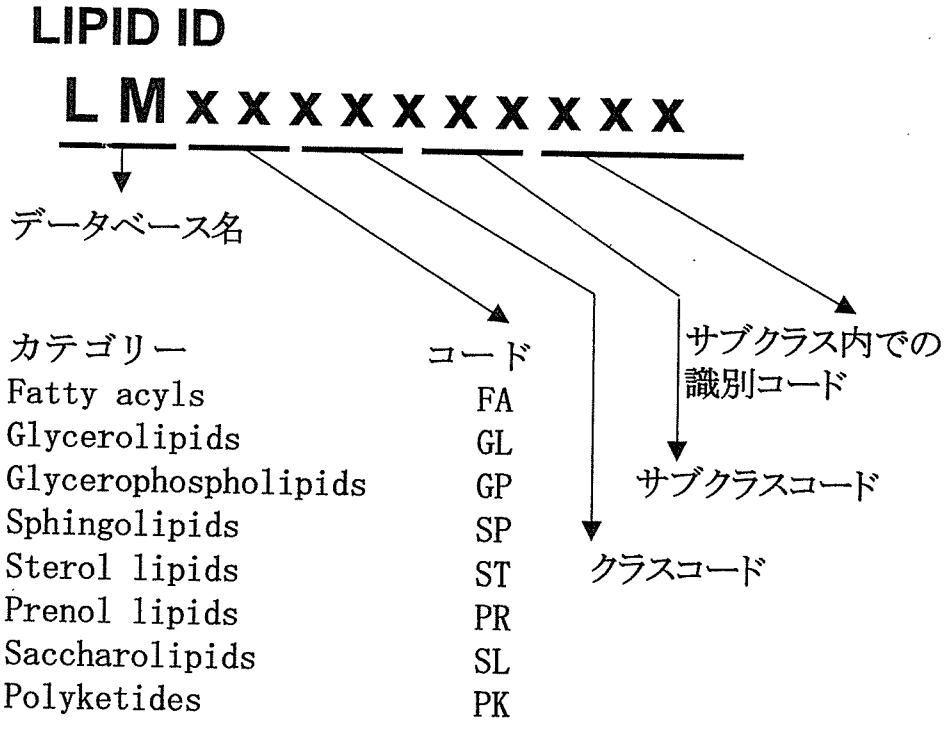

データベース名
LM, LIPID MAPS (http://www.lipidmaps.org)

図2

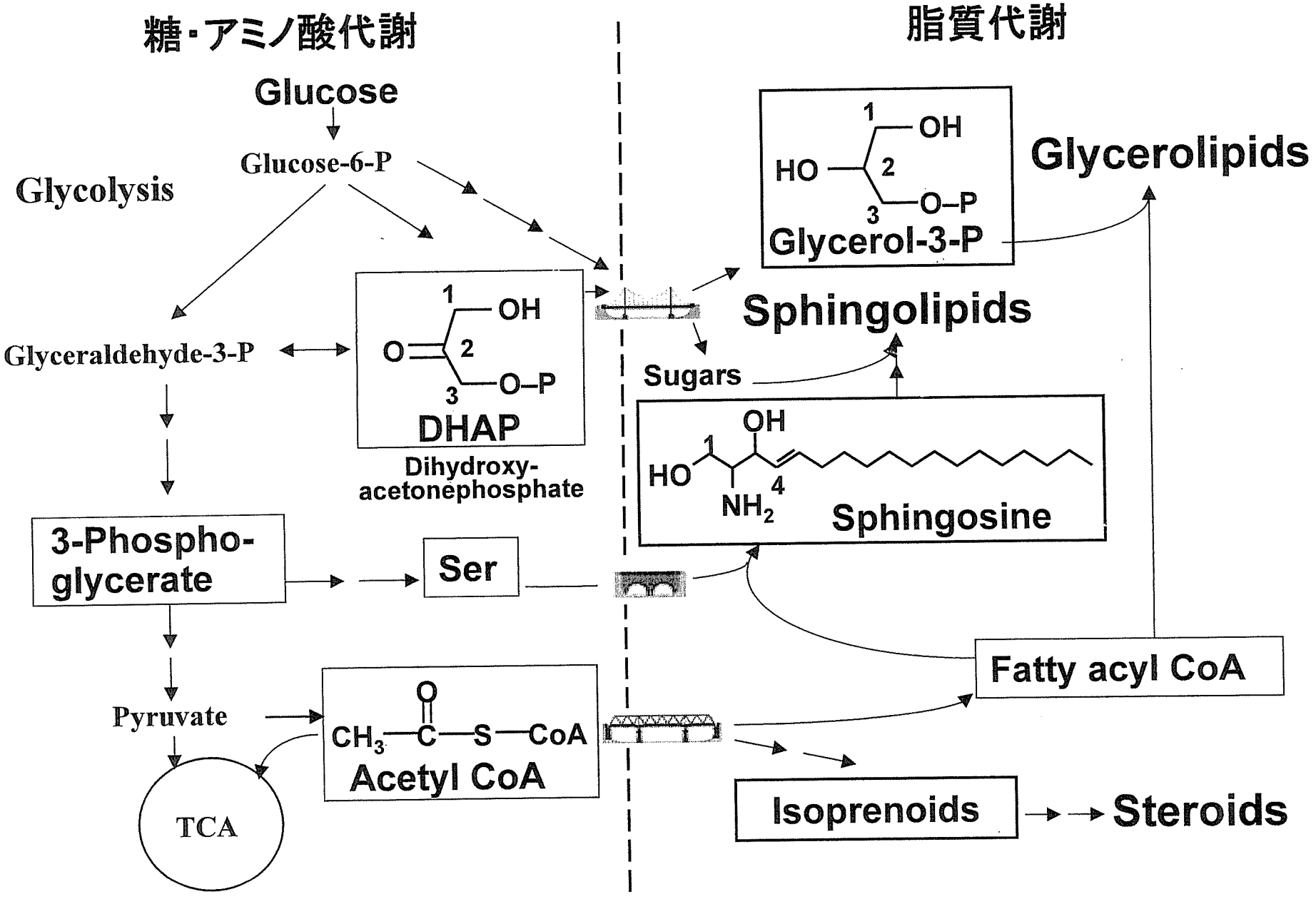
糖・アミノ酸代謝
脂質代謝
Glucose
Glucose-6-P
Glycolysis
Glycerolipids
Glycerol-3-P
Glyceraldehyde-3-P
DHAP
Dihydroxy-
acetonephosphate
Sphingolipids
Sugars
Sphingosine
3-Phospho-
glycerate
Ser
Fatty acyl CoA
Pyruvate
Acetyl CoA
TCA
Isoprenoids
Steroids

図3

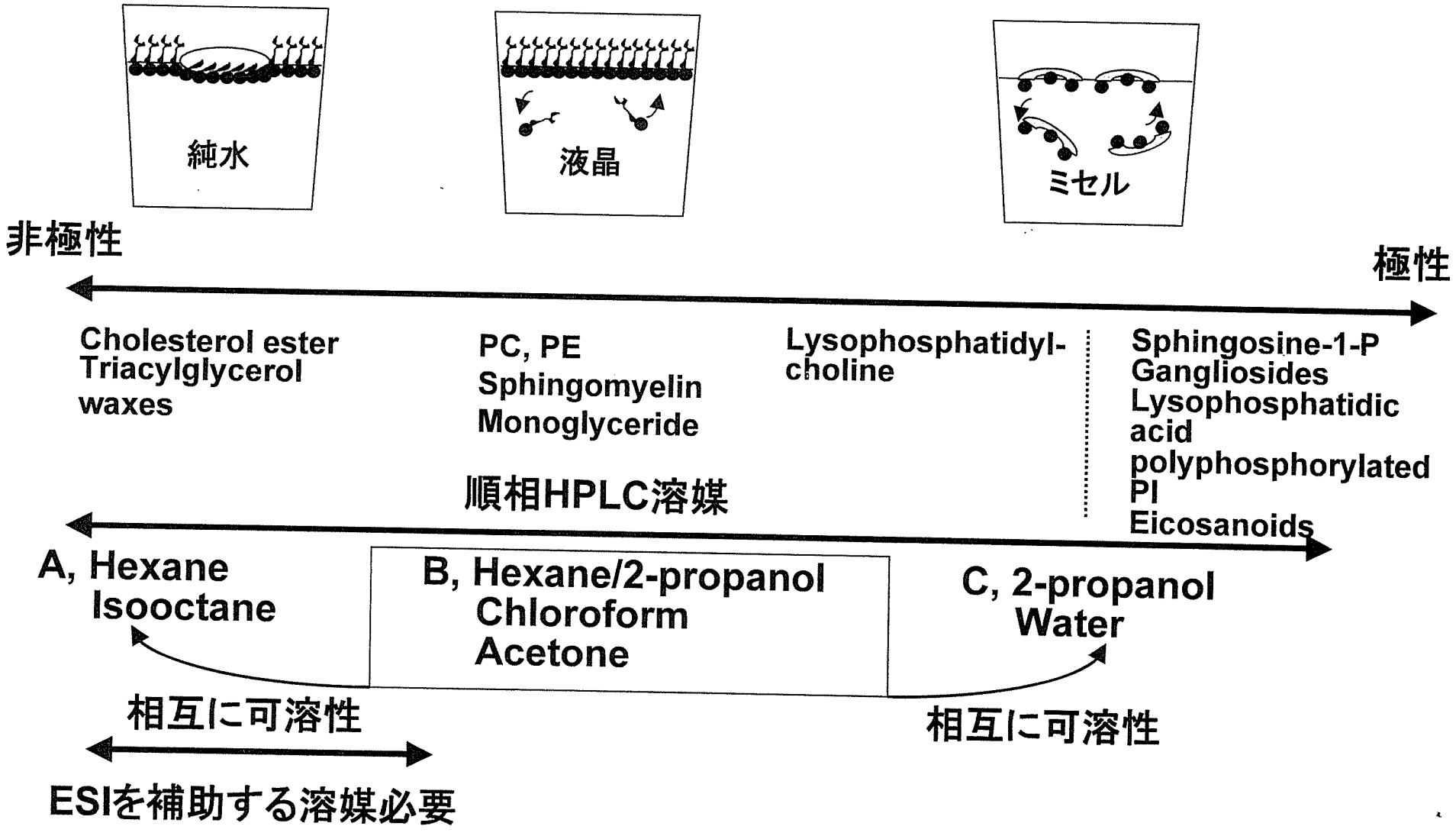
純水
液晶
ミセル
非極性
極性
Cholesterol ester
Triacylglycerol
waxes
PC, PE
Sphingomyelin
Monoglyceride
Lysophosphatidyl-
choline
Sphingosine-1-P
Gangliosides
Lysophosphatidic
acid
polyphosphorylated
PI
Eicosanoids
順相HPLC溶媒
A, Hexane
Isooctane
B, Hexane/2-propanol
Chloroform
Acetone
C, 2-propanol
Water
相互に可溶性
相互に可溶性
ESIを補助する溶媒必要

図4

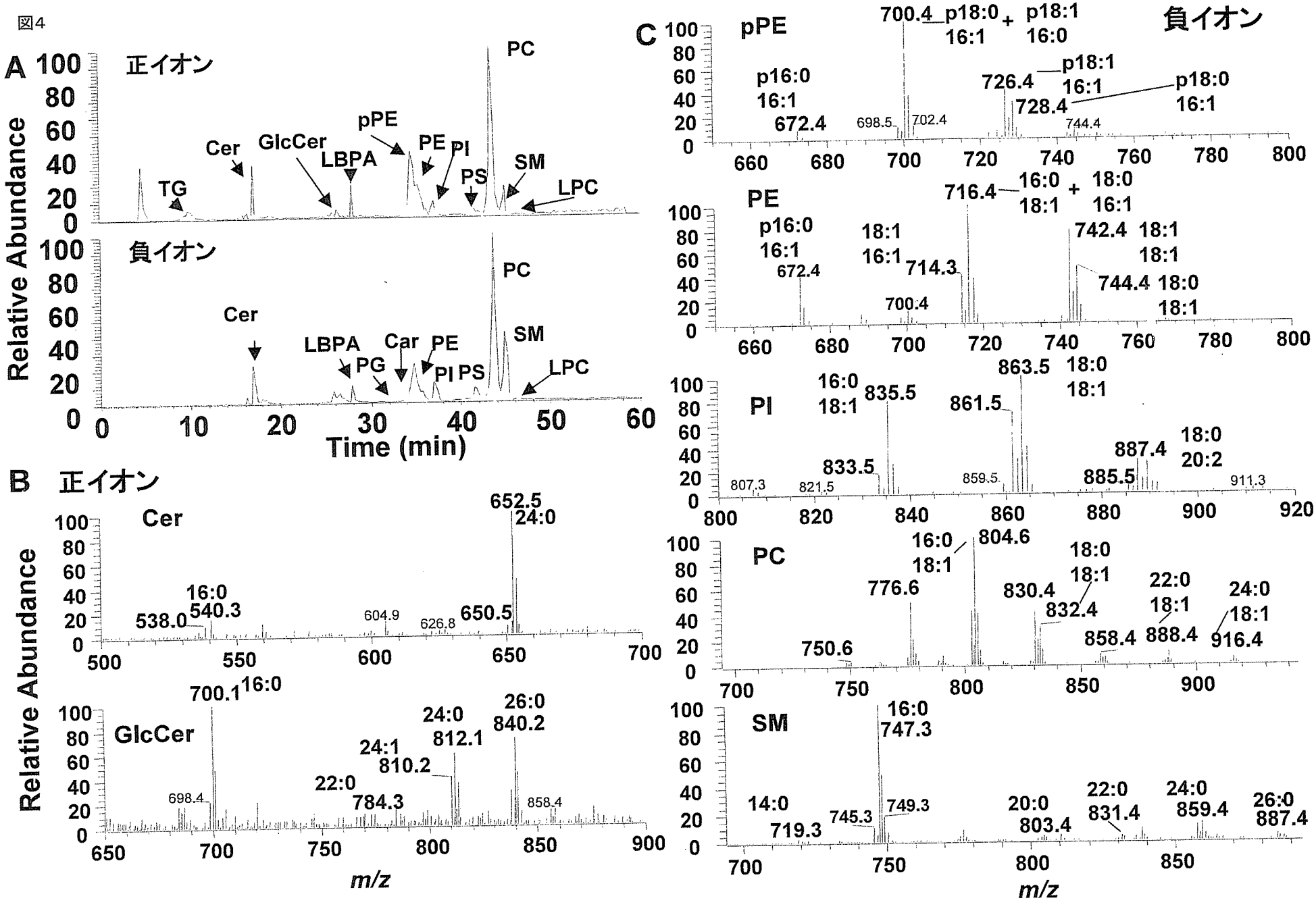
A
正イオン
負イオン
Relative Abundance
Time (min)
TG
Cer
GlcCer
LBPA
pPE
PE
PI
PS
PC
SM
LPC
Car
PG
B
正イオン
Cer
652.5
24:0
16:0
540.3
538.0
604.9
626.8
650.5
GlcCer
700.1
16:0
24:0
812.1
26:0
840.2
24:1
810.2
22:0
784.3
698.4
858.4
m/z
C
負イオン
pPE
700.4
p18:0
16:1
+
p18:1
16:0
p16:0
16:1
672.4
698.5
702.4
726.4
p18:1
16:1
728.4
p18:0
16:1
744.4
PE
716.4
16:0
18:1
+
18:0
16:1
p16:0
16:1
672.4
18:1
16:1
714.3
700.4
742.4
18:1
18:1
744.4
18:0
18:1
PI
863.5
18:0
18:1
16:0
18:1
835.5
861.5
833.5
807.3
821.5
859.5
887.4
18:0
20:2
885.5
911.3
PC
804.6
16:0
18:1
18:0
18:1
776.6
830.4
832.4
22:0
18:1
24:0
18:1
750.6
858.4
888.4
916.4
SM
16:0
747.3
14:0
719.3
745.3
749.3
20:0
803.4
22:0
831.4
24:0
859.4
26:0
887.4
m/z

Demonstration of Aqueous Streaming Through a Laser Iridotomy Window Against the Corneal Endothelium

Yasuaki Yamamoto, MD; Toshihiko Uno, MD, PhD; Katsumi Shisida, MD; Longquan Xue, MD; Atsushi Shiraishi, MD, PhD; Xiaodong Zheng, MD, PhD; Yuichi Ohashi, MD, PhD

Objective: To determine the pathogenesis of the bullous keratopathy that is frequently observed in patients after argon laser iridotomy (ALI) by comparing the changes in aqueous flow after ALI with those that follow peripheral iridectomy in rabbit eyes.

Methods: Silicone particles were injected into the anterior chamber of rabbit eyes as tracers to monitor aqueous flow. Particle tracking velocimetry with image analysis was used to determine the direction and speed of aqueous flow in 5 pigmented rabbits that underwent ALI and 5 that underwent peripheral iridectomy.

Results: In the ALI group, silicone particles were found to stream through the iridotomy window against the corneal endothelium immediately after the pupil was constricted by a light stimulus. The mean±SD speed of the particles was 2.97±1.51 mm/s. In contrast, the mean±SD flow rate through the iridectomy window in the peripheral iridectomy group was significantly slower at 0.36±0.30 mm/s (P=.01).

Conclusion: Constriction of the pupil elicited marked aqueous streaming through the ALI window against the corneal endothelium.

Clinical Relevance: The mechanical stress to the corneal endothelium by the abnormal aqueous stream may be partially responsible for the corneal decompensation that follows ALI.

Arch Ophthalmol. 2006;124:387-393

ARGON LASER IRIDOTOMY (ALI) has been widely used for the prevention and treatment of angle closure glaucoma since its introduction into clinical practice by Quigley[1] in 1981. In 1984, Pollack[2] reported the first case of irreversible corneal edema after ALI, and in 1988, Schwartz et al[3] reported more cases of phakic bullous keratopathy and concluded that corneal edema was a serious complication of ALI. The incidence of this devastating disorder is increasing yearly, and, in Japan, ALI-induced bullous keratopathy is now recognized as the second most common corneal disease requiring penetrating keratoplasty to restore good visual acuity.[2-11]

A variety of causes have been postulated for bullous keratopathy, for example, excessive laser irradiation,[3,4,7-9,11] a history of acute glaucomatous attack,[3,5,6,8,10,11] diabetes mellitus,[3,6,8,11] and abnormalities in the corneal endothelium, such as cornea guttata and Fuchs corneal degeneration.[3,6,7-9,11] However, these factors do not fully explain the pathogenetic mechanism in most cases.

We hypothesize that changes in the dynamics of the flow of aqueous humor are related to the corneal endothelial decompensation that follows ALI. To date, the dynamic changes in aqueous flow in the anterior chamber have not been studied in detail because aqueous flow is not visible except when inflammatory cells are present in the anterior chamber. Recent improvements in imaging devices and computer techniques now allow the use of principles developed for particle tracking velocimetry (PTV) to detect the flow of the aqueous humor.[12,13] Using silicone powder as a tracer, we quantitatively analyzed changes in the direction and speed of aqueous flow and compared the velocity and course of aqueous flow after ALI vs after peripheral iridectomy (PI) in rabbits.

Author Affiliations:
Departments of Ophthalmology, Ehime University, Shitsukawa, Toon-city, Ehime (Drs Yamamoto, Uno, Shisida, Xue, Shiraishi, Zheng, and Ohashi), and Takanoko Hospital, Matsuyama City (Drs Yamamoto and Shiraishi), Japan.

METHODS

ANIMALS AND TRACER

Healthy Dutch pigmented rabbits (weight, 1.5-2.5 kg) were used. All the procedures were performed under general anesthesia with an intramuscular injection of 5% ketamine

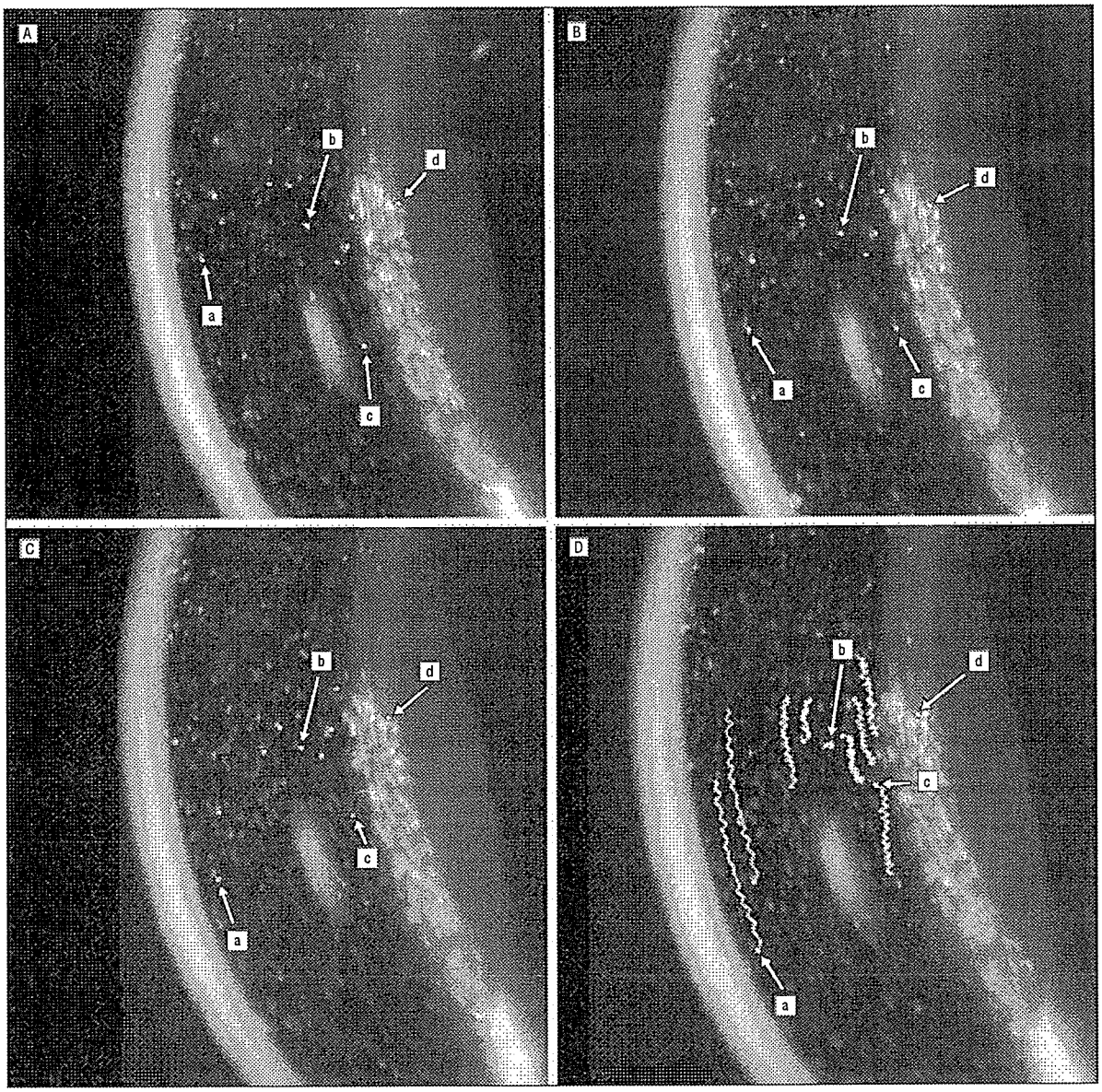

Figure 1. Still photographs of particles in the anterior chamber at 0 (A), 3 (B), 5 (C), and 8 (D) seconds showing a descending particle (a), the center of the circular current (b), and an ascending particle (c). Particles attached to the surface of the lens are used to track the movement of the rabbit (d). The wavy lines in D indicate the track of each particle.

hydrochloride, 25 mg/kg (Ketalar; Sankyo-Yell, Tokyo, Japan), and xylazine hydrochloride, 5 mg/kg (Celactar; Bayer, Tokyo), and under topical corneal anesthesia with 0.4% oxybuprocaine hydrochloride ophthalmic solution. In managing the rabbits, we adhered strictly to the Guiding Principles in the Care and Use of Animals (US Department of Health, Education, and Welfare publication NIH 80-23).

Silicone powder (KMP-602; Shin-Etsu Chemical Co Ltd, Tokyo), consisting of homogeneous particles with a mean diameter of 30 μm and specific gravity of 0.98, was used as a tracer to make aqueous flow visible.

EXPERIMENTAL DESIGN

Fifteen rabbits were randomly separated into 3 equal groups. One group served as controls without treatment, the second group underwent unilateral ALI, and the third group underwent unilateral PI. The rabbits in the ALI and PI groups were monitored for more than 2 weeks until the inflammatory reactions induced by the surgical procedures were completely resolved.

To examine the pattern and velocity of aqueous flow, 0.05 g of silicone powder was suspended in 10 mL of isotonic sodium chloride solution. Then, 0.2 mL of the suspension was injected through a corneal limbal incision at the 2-o'clock position using a 30-gauge needle on a 1-mL disposable syringe. All the rabbits were allowed to recover for at least 15 minutes after the injection, until the movements of the silicone particles became consistent. Then, the movements of the silicone particles were videotaped and analyzed using PTV.

In the control group, the speed of the thermal current was quantitatively analyzed, and in the ALI and PI groups, the movement of the tracer particles in the vicinity of the iridotomy or

iridectomy window was also measured. To induce pupillary constriction, the width of the slit beam was increased from 0.3 to 2.0 mm. Changes in aqueous flow were monitored before and during miosis. The speed of flow of the aqueous from the posterior chamber through the opening in the iris into the anterior chamber was compared in the 2 groups.

EXAMINATION OF AQUEOUS FLOW AND PTV

Movement of the silicone particles into the anterior chamber was observed by using a slitlamp biomicroscope and was recorded on videotape by using a charge-coupled device camera. The slit beam was aligned with the center of the cornea and projected vertically onto the anterior surface of the lens. The angle between the observer's eye and the slit beam was maintained at 60°.

The images of the movement of the particles on the videotape were transferred to a personal computer, and the flow speed was determined by monitoring the displacement of individual particles using image analysis software (Image Tracker PTV 2001; Digimo Co Ltd, Osaka, Japan). The images were first converted into still pictures at 30 frames per second, and the coordinates of selected particles were determined for each frame. Then, regression lines were calculated based on the sequential changes of the coordinates of each particle. The speed of flow of the particles was calculated from the slope of each regression line.

Because the coordinates of the particles also changed from movements of the rabbit, the coordinates of each particle were corrected by subtracting the coordinates of particles that were adherent to the surface of the lens or corneal endothelium from those of the individual particles floating in the aqueous humor.

SURGICAL PROCEDURES FOR ALI AND PI

The multicolor laser photocoagulater (Novus Omni; Coherent, Inc, Santa Clara, Calif) was used for ALI. The 2-step long-burn technique using the Abraham lens was used: 8 stretching burns with 521 nm of argon green, 200-μm spot size, 0.2 second, and 200 mW of power followed by 272 to 432 penetrating burns with 521 nm of argon green, 50-μm spot size, 0.02 second, and 1000 mW of power. For PI, the iris was pulled out of a limbal incision and resected to produce an iridectomy diameter of approximately 3.0 mm at the 12-o'clock position. The prolapsed iris was gently repositioned using a spatula to avoid any incarceration in the incision site. Finally, the wound was closed using a single 10-0 nylon suture.

RESULTS

The silicone particles were well dispersed in the aqueous humor without any aggregation. Some particles were adherent to the corneal endothelium and the anterior surface of the lens and iris, but most were seen to be moving along with the aqueous flow.

AQUEOUS FLOW IN THE ANTERIOR CHAMBER

Control Group

Slitlamp examination showed continuous movement of the particles in a circular path, with a descending flow near the corneal endothelium and an ascending flow near the anterior surface of the iris. This pattern is consistent with the theory of the thermal current of the aqueous humor in the anterior chamber[14] (**Figure 1**). Changes in the coordinates of 19 particles in 5 rabbit eyes were plotted. The graph of 1 descending particle in the vicinity of the corneal endothelium is shown in **Figure 2**. The mean±SD flow speeds were 0.180±0.056 mm/s for the descending flow near the corneal endothelium and 0.068±0.015 mm/s for the ascending flow near the anterior surface of the lens.

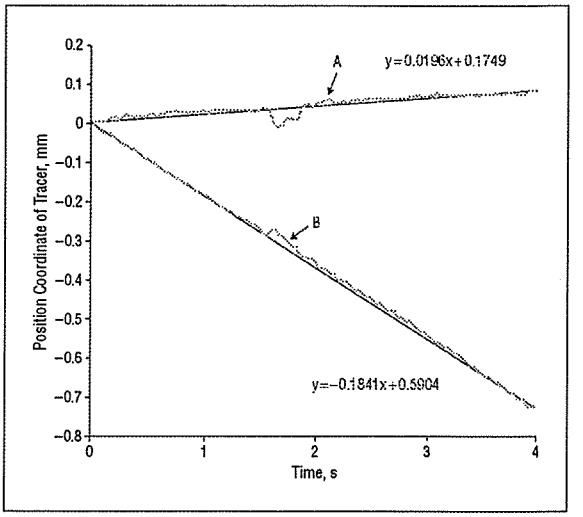

Figure 2. Changes in the coordinates of the movement of 1 descending particle in the vicinity of the corneal endothelium. Position "0" represents the starting position of the particle in the anterior chamber. A shows the changes in the coordinates from the cornea to the iris. B represents the particle position from top to bottom. Flow speed is calculated from the slope of the regression line.

ALI Group

The pattern of thermal flow of the particles was almost the same as in control eyes. However, when the pupil was constricted, a stream of particles was seen to flow into the anterior chamber from the posterior chamber through the iridotomy window. After the pupil dilated, the particles were drawn back into the posterior chamber through the iridotomy window. The tracking images of these particles, plotted by monitoring individual particles for 1 second, are shown in **Figure 3** and **Figure 4**. The streaming particles were seen to collide against the corneal endothelium and then move downward in the anterior chamber (arrows in Figure 3).

PI Group

In the PI group, particles were seen to descend not only near the cornea but also along the anterior surface of the lens. The ascending particles were seen near the surface of the iris when the slit beam was shifted laterally. Constriction of the pupil accelerated the speed of the descending particles near the iridectomy window to some extent, but no particles were seen to collide with the corneal endothelium. The tracking images of these particles, plotted for 1 second, are shown in **Figure 5**.

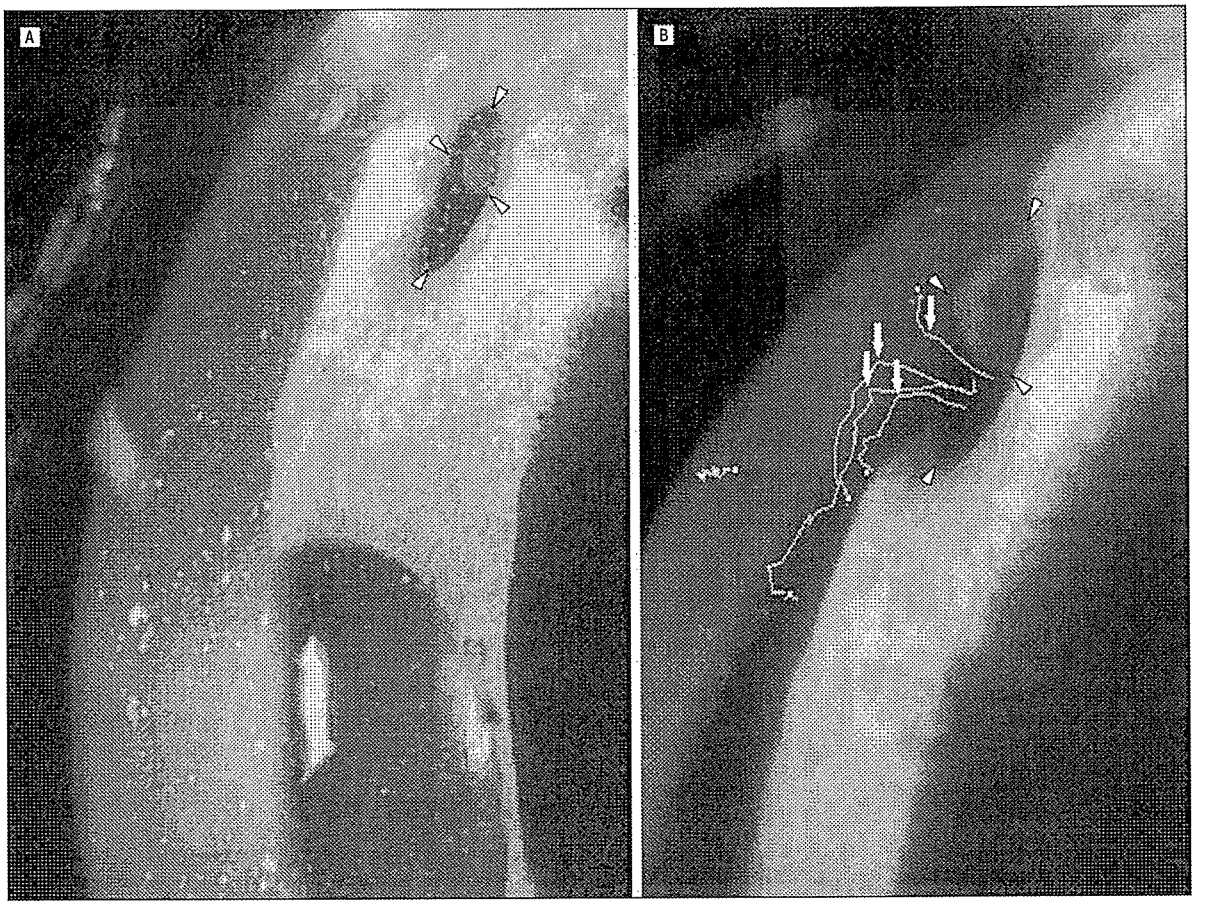

Figure 3. Photograph demonstrating aqueous streaming into the anterior chamber from the posterior chamber through the argon laser iridotomy (ALI) window. A, An eye with ALI during pupil constriction (when the slit beam was increased). B, At that time, the tracking images of streaming particles are indicated in the higher view of the vicinity of the iridotomy window (arrowheads). The particles collided against the corneal endothelium (arrows). The wavy lines indicate the track of each particle.

COMPARISON OF FLOW THROUGH THE OPEN WINDOW IN THE IRIS AFTER MIOSIS IN BOTH GROUPS

The speed of the particles streaming through the opening in the ALI and PI group during a 0.1-second period after miosis is plotted in **Figure 6**. The mean±SD flow speed of the 25 particles in the ALI group was 2.97±1.51 mm/s, whereas that of the 25 particles in the PI group was 0.36±0.30 mm/s. This difference in the mean flow speed was significant ($P=.01$, by Mann-Whitney test). The size of the iris window was measured on the images downloaded to the computer. The mean±SD area of laser iridotomy in the ALI group was 0.96±0.31 mm^2, whereas that in the PI group was 5.84±2.12 mm^2. The difference in the areas of the iris window between the 2 groups was significant ($P=.006$, by Mann-Whitney test).

COMMENT

We succeeded in "seeing" the flow of aqueous humor in the anterior chamber of rabbit eyes by using silicone powder as a tracer. The technique of PTV was then used to determine the direction and speed of the particles. Our results confirm the presence of a thermal current of aqueous humor in the anterior chamber. As stated, the accuracy of the velocity measurement by PTV is ultimately determined by the ability of the scattering particles to follow the instantaneous motion of the fluid.

In this sense, careful selection of a tracer particle is critical, and several properties should be present in the particles. First, the tracer particles must be large enough to have good light-scattering ability and to be detected by a video camera so that digitized data can be analyzed. Second, the tracer particle should be small enough to be carried passively with the current of the fluid. An ideal tracer particle would have a specific gravity identical to that of the aqueous humor. And third, the particle should be nontoxic, noncorrosive, and chemically inert. With respect to these requirements, many studies have used particles with diameters ranging from 2 to 500 μm and density ratios of 0.7 to 1.05.[15] Silicone powder has these properties and thus was used in this study.

The exact cause of the corneal endothelial decompensation that follows ALI has not been determined. For example, excessive laser irradiation can cause serious endothelial damage, but we seldom see such a

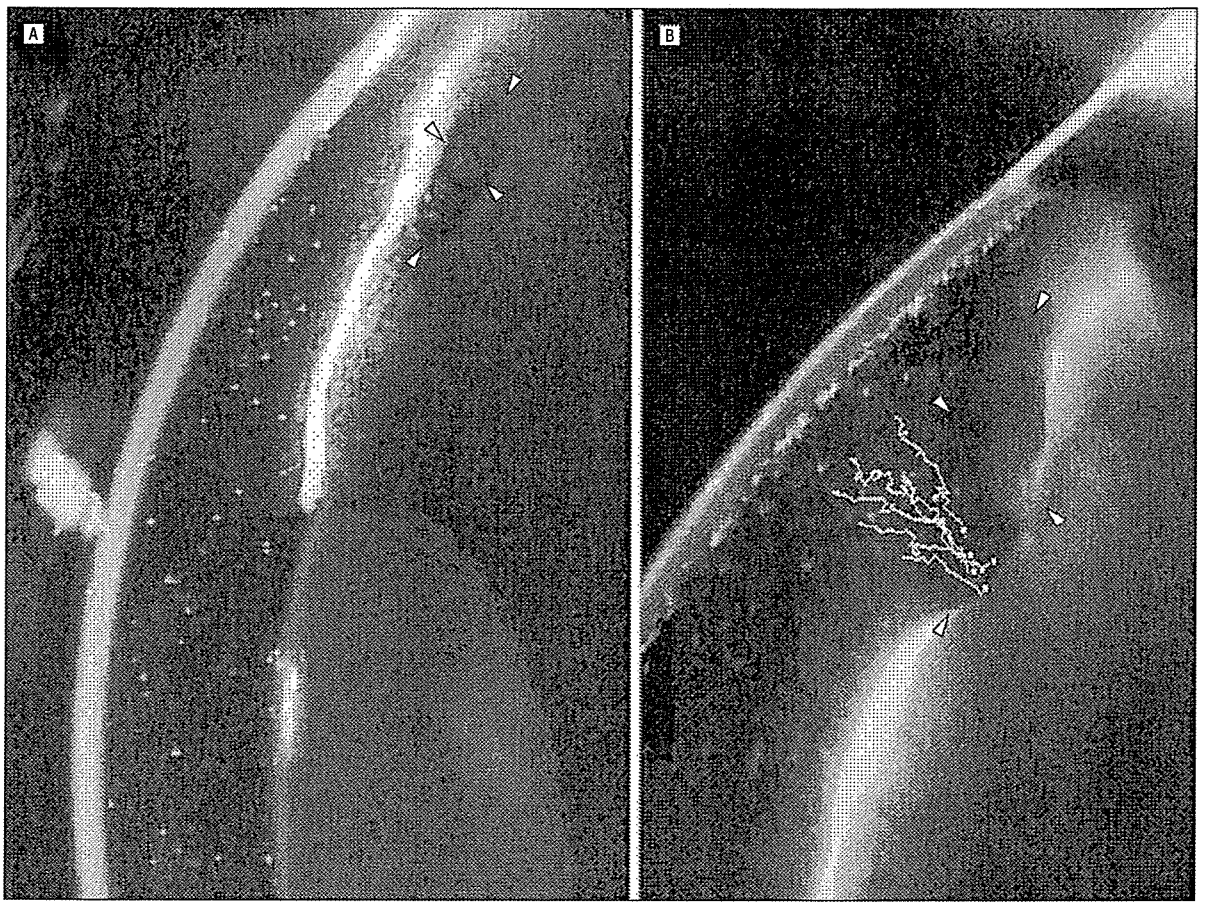

Figure 4. Photograph demonstrating the drawn-back flow into the posterior chamber through the argon laser iridotomy (ALI) window. A, An eye with ALI during dilation of the pupil (when the slit beam was narrowed). B, At that time, the tracking images of particles flow back into the posterior chamber and are indicated by the higher view in the vicinity of the iridotomy window (arrowheads). The wavy lines indicate the track of each particle.

patient develop severe corneal edema immediately after surgery. In addition, corneal endothelial decompensation can develop even after uneventful laser procedures. Although a history of acute glaucomatous attack is a risk factor for corneal endothelial decompensation, irreversible bullous keratopathy almost never develops in eyes that undergo surgical iridectomy. The presence of diabetes mellitus or corneal endothelial abnormalities, such as cornea guttata or Fuchs corneal dystrophy, has not been associated with many cases of bullous keratopathy.

Our most striking finding was the presence of aqueous streaming through the small opening of the iris after ALI. This showed that laser iridotomy causes an extremely fast forward aqueous flow, which occurs through the iris window during miosis, followed by the backward flow as the pupil dilates. The mean speed of this streaming from the posterior chamber to the anterior chamber was estimated to be 2.97 mm/s, which is approximately 17 times faster than the ordinary thermal current. More important, the stream was directed against the corneal endothelium, unlike the direction of the physiologic thermal current, which flows parallel to the corneal endothelium. Just as the continuous shear stress of vascular flow on vascular endothelial cells has gained attention as a causative mechanism in arteriosclerosis or aneurysm formation,[16-18] such an abnormal stream can be suggested to damage corneal endothelial cells. If this streaming is repeated in response to light stimuli for long periods, the corneal endothelial cells around the window may be damaged, leading to corneal endothelial cell dysfunction.

In contrast to the stream observed in the ALI group, the flow speed through a large-diameter surgical iridectomy in the PI group was found to be slow and not directed against the corneal endothelium. This may explain the fewer cases of endothelial dysfunction observed in patients after standard surgical PI, a procedure widely performed before the development of ALI.

Corneal endothelial dysfunction occurs predominantly after ALI but also rarely after Nd:YAG laser iridotomy. One may argue that such corneal endothelial decompensation can be avoided if an Nd:YAG laser is applied to make an iris opening because the thermal effect is thought to be substantially reduced using this procedure. However, it has been reported that the dysfunction can develop in patients after laser iridotomy using an Nd:YAG laser.[7,9,19,20] Therefore, it seems that the thermal damage to the corneal endothelium elicited by the ALI procedure cannot be the only causative factor, and

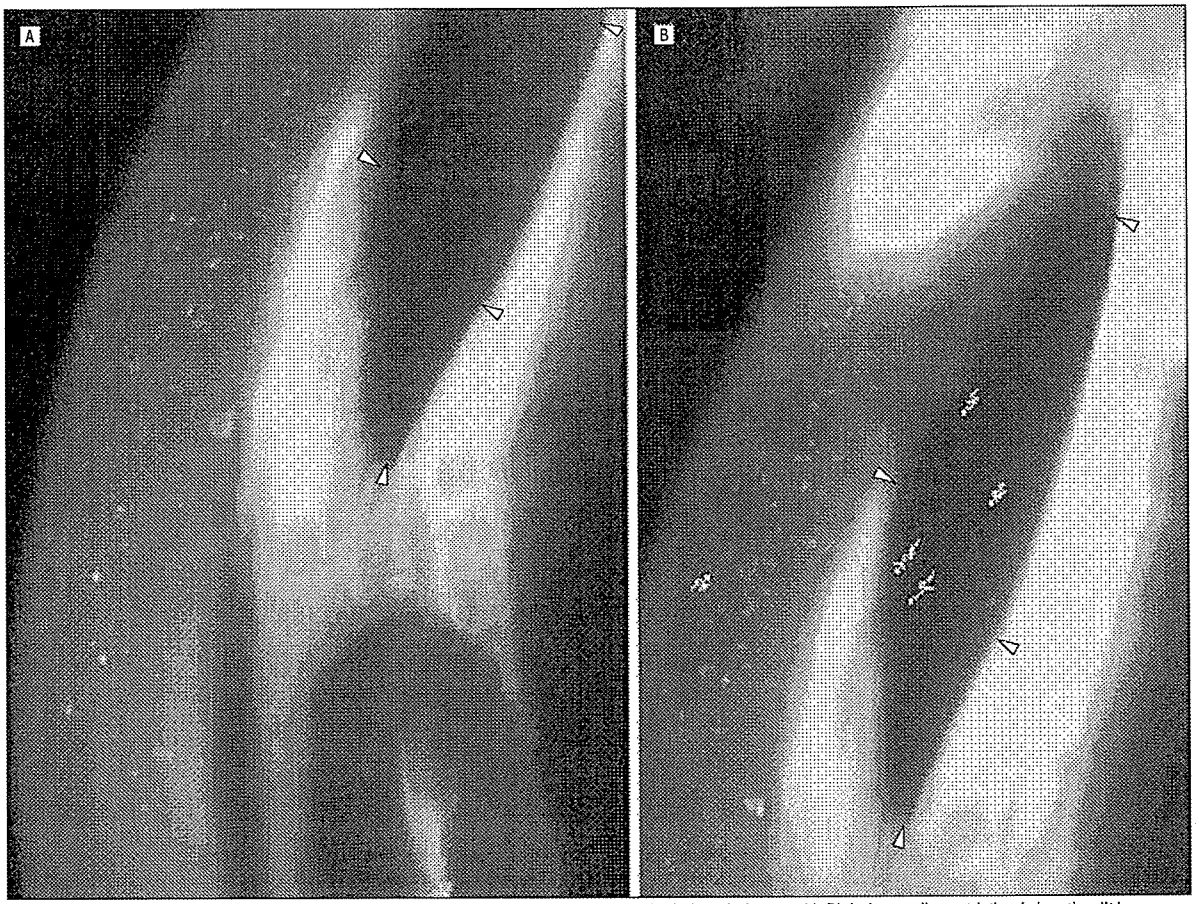

Figure 5. Photograph demonstrating the aqueous flow through the peripheral iridectomy (PI) window. A, An eye with PI during pupil constriction (when the slit beam was increased). B, At that time, the tracking images of particles are indicated by the higher view in the vicinity of the iridectomy window (arrowheads). None of the particles were noted to collide with the corneal endothelium. The wavy lines indicate the track of each particle.

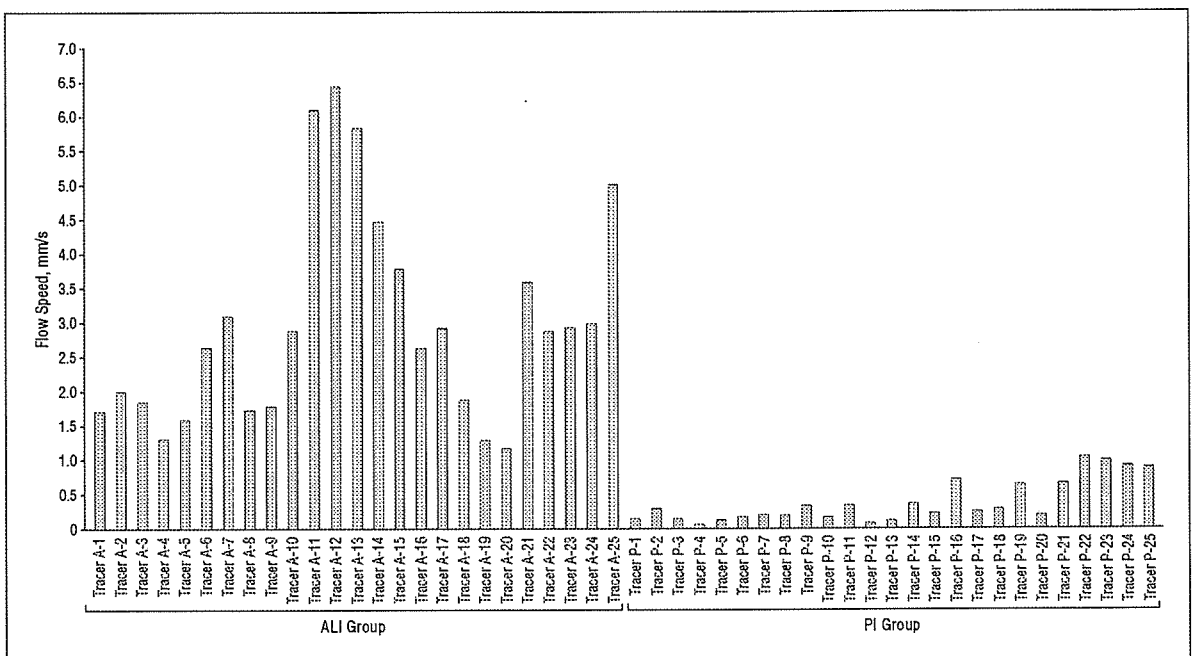

Figure 6. The speed of the particles streaming through the opening in the argon laser iridotomy (ALI) and peripheral iridectomy (PI) groups during a 0.1-second period after miosis. The mean±SD flow speed in the ALI group was 2.97±1.51 mm/s and in the PI group was 0.36±0.30 mm/s (P=.01, by Mann-Whitney test).

the importance of the changes in aqueous flow should be considered.

This type of unusual streaming should be present in all patients to some degree; however, corneal endothelial dysfunction develops in few patients. Possible explanations for this discrepancy include differences in the size of the iridotomy, the location of the window, the distance between the window and the corneal endothelium, and the presence or absence of posterior synechia. These factors are intricately intertwined, and few patients will experience serious corneal endothelial dysfunction that leads to irreversible bullous keratopathy.

Why does such streaming occur? Generally, during miosis, the pressure in the posterior chamber rises, which leads to the flow of aqueous into the anterior chamber. As the pupil and the central region of the posterior surface of the iris make appositional contact with the anterior surface of the lens and retard aqueous flow, the rapid release of the pressure should result in the aqueous stream when the opening is small.

Because the aqueous humor plays an essential role in maintaining the homeostasis of the anterior segment of the eye, any changes may have a profound effect and could be associated with a variety of ocular disorders. In this regard, the method of making aqueous flow visible described herein can be used to analyze changes in its dynamics and could possibly contribute to the further understanding of the pathogenesis of anterior segment disorders.

Submitted for Publication: April 20, 2005; accepted July 15, 2005.
Correspondence: Yasuaki Yamamoto, MD, Department of Ophthalmology, Ehime University, Shitsukawa, Toon-city, Ehime, Japan (yyasuaki@m.ehime-u.ac.jp).
Financial Disclosure: None.

REFERENCES

1. Quigley HA. Long-term follow-up of laser iridotomy. *Ophthalmology.* 1981;88:218-224.
2. Pollack IP. Current concepts in laser iridotomy. *Int Ophthalmol Clin.* 1984;24:153-180.
3. Schwartz AL, Martin NF, Weber PA. Corneal decompensation after argon laser iridectomy. *Arch Ophthalmol.* 1988;106:1572-1574.
4. Hong C, Kitazawa Y, Tanishima T. Influence of argon laser treatment of glaucoma on corneal endothelium. *Jpn J Ophthalmol.* 1983;27:567-574.
5. Zabel RW, MacDonald IM, Minstsioulis G. Corneal endothelial decompensation after argon laser iridotomy. *Can J Ophthalmol.* 1991;26:367-373.
6. Jeng S, Lee JS, Haung SCM. Corneal decompensation after argon laser iridotomy: a delayed complication. *Ophthalmic Surg.* 1991;22:565-569.
7. Wilhelmus KR. Corneal edema following argon laser iridotomy. *Ophthalmic Surg.* 1992;23:533-538.
8. Yuguchi M, Nagasaka M. Bullous keratopathy following argon laser iridotomy. *Jpn J Clin Ophthalmol.* 1992;86:2098-2101.
9. Hosotani H, Ohashi Y, Ohguro N, Kuwayama Y, Knoshita S. Corneal endothelial decompensation after argon laser iridotomy. *Jpn J Clin Ophthalmol.* 1994; 48:420-422.
10. Ishimura H, Kono M, Nakamura J. Bullous keratopathy following argon laser iridotomy. *Jpn J Clin Ophthalmol.* 1997;51:1123-1126.
11. Kanai H, Sotozono C, Komuro A, et al. Bullous keratopathy following argon laser iridotomy. *Atarashii Ganka.* 2003;20:245-249.
12. Adrian RJ. Particle-imaging techniques for experimental fluid mechanics. *Annu Rev Fluid Mech.* 1991;23:261-304.
13. Adrian RJ. Bibliography of particle velocimetry using imaging methods. *TAM Rep.* 1996;817:1917-1995.
14. Duke-Elder S, Gloster J, Weale R. The circulation of the aqueous humour. In: *Physiology of the Eye and of Vision.* St Louis, Mo: CV Mosby; 1968;V:118-130.
15. Melling A. Tracer particles and seeding for particle image velocimetry. *Meas Sci Technol.* 1997;8:1406-1416.
16. Ku DN, Giddens DP, Zarins CK, Glagov S. Pulsatile flow and atherosclerosis in the human carotid bifurcation. *Arteriosclerosis.* 1985;5:293-301.
17. Nerem RM, Harrison DG, Taylor WR, Alexander RW. Hemodynamics and vascular endothelial biology. *J Cardiovasc Pharmacol.* 1993;21:S6-S10.
18. Ujiie H, Tachibana H, Kajiya F, et al. Effect of size and shape (aspect ratio) on the hemodynamics of saccular aneurysms: a possible index for surgical treatment of intracranial aneurysms. *Neurosurgery.* 1999;45:119-130.
19. Panek WC, Lee DA, Christensen RE. The effects of Nd:YAG laser iridotomy on the corneal endothelium. *Am J Ophthalmol.* 1991;111:505-507.
20. Wu SC, Jeng S, Huang SCM, Lin SM. Corneal endothelial damage after neodymium: YAG laser iridotomy. *Ophthalmic Surg Lasers.* 2000;31:411-416.

Current Eye Research, 31:129–136, 2006

ISSN: 0271-3683 print / 1460-2202 online
DOI: 10.1080/02713680500507200

Taylor & Francis
Taylor & Francis Group

Role of Angiotensin II Receptor Subtypes in Conjunctival Wound Healing

Shiro Mizoue
Department of Ophthalmology, and Department of Molecular and Cellular Biology, Division of Medical Biochemistry and Cardiovascular Biology, Ehime University School of Medicine, Ehime, Japan

Masaru Iwai, Ayumi Ide, Jun Suzuki, and Masatsugu Horiuchi
Department of Molecular and Cellular Biology, Division of Medical Biochemistry and Cardiovascular Biology, Ehime University School of Medicine, Ehime, Japan

Atsushi Shiraishi and Yuichi Ohashi
Department of Ophthalmology, Ehime University School of Medicine, Ehime, Japan

ABSTRACT *Purpose*: To investigate the role of angiotensin II (Ang II) receptor subtypes in subconjunctival injury. *Methods*: A wound-healing model was developed by subconjunctival blunt dissection in male wild-type, AT_{1a} receptor–deficient ($AT_{1a}KO$) and AT_2 receptor–deficient (AT_2KO) mice. Collagen deposition and cell infiltration were evaluated histologically. Expression of collagen, matrix metalloproteinase (MMP), and tissue inhibitor of metalloproteinase-1 (TIMP-1) were determined by real-time PCR. *Results*: Subconjunctival injury increased the infiltration of inflammatory cells, collagen deposition in the subconjunctival space, and the expression of collagen type I and type III, TIMP-1 and MMP2. In $AT_{1a}KO$ mice, collagen deposition, cell infiltration, and expression of collagen and TIMP-1 were inhibited, but MMP2 expression was enhanced. In contrast, in AT_2KO mice, the increase in collagen deposition, cell infiltration, and expression of collagen and TIMP-1 were further enhanced. *Conclusions*: These results indicate that AT_{1a} and AT_2 receptor stimulation may in addition to other mechanisms be antagonistically involved in the wound-healing process after subconjunctival injury.

KEYWORDS angiotensin II; collagen; conjunctiva; transgenic mouse; wound healing

INTRODUCTION

The conjunctival wound-healing reaction seems to play a key role in the results of surgery for glaucoma[1] or pterygium[2] and ocular surface reconstruction.[3] However, the mechanism of the conjunctival wound-healing reaction has not been fully elucidated despite its clinical importance.

Angiotensin II (Ang II) regulates wound healing in the skin, as well as cardiovascular structure and hemodynamics, through type 1 (AT_1) and type 2 (AT_2) receptors.[4–7] Fibroblasts and phenotypically transformed myofibroblasts[8] play a critical role in cardiac remodeling through extracellular matrix (ECM) protein deposition and both matrix metalloproteinase (MMP) and tissue inhibitor of metalloproteinase-1 (TIMP-1) production.[9] It has been reported that AT_1 receptor stimulation induces cell proliferation and accumulation of ECM.[4] On the other hand, AT_2 receptor stimulation has shown antagonistic actions against AT_1 receptor stimulation in various experiments.[4,10,11] Because it is reported that both AT_1 and AT_2 receptors are expressed in the eye,[12] it seems probable that these receptors play a critical role in the wound-healing process in ocular

Received 24 August 2004
Accepted 15 February 2005

Correspondence: Masatsugu Horiuchi, M.D., Ph.D., Department of Molecular and Cellular Biology, Division of Medical Biochemistry and Cardiovascular Biology, Ehime University School of Medicine, Shitsukawa, Shigenobu, Onsen-gun, Ehime 791-0295, Japan. E-mail: horiuchi@m.ehime-u.ac.jp

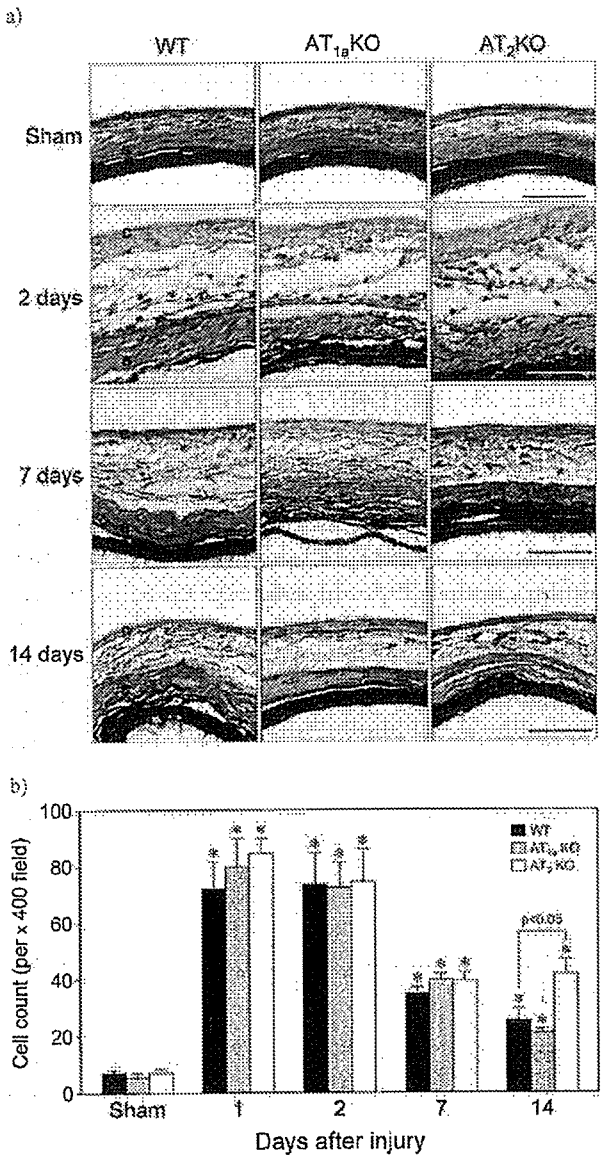

FIGURE 1 Histological changes in subconjunctival tissue in AT_2KO and $AT_{1a}KO$ mice after subconjunctival injury. Subconjunctival injury was induced and cross sections of eye samples were prepared as described in "Materials and Methods." (a) Representative cross sections of injured eyes with hematoxylin and eosin staining. (C, conjunctiva; S, sclera. Magnification, ×400; scale bar, 50 μm.) (b) Changes in total cell count in subconjunctival space after injury. Total cells in the subconjunctival space were counted using a cross section of the eye as described in "Materials and Methods." (Sham, sham operation.) *$p < 0.05$ versus sham group. Values are mean ± SEM of 4 to 6 animals.

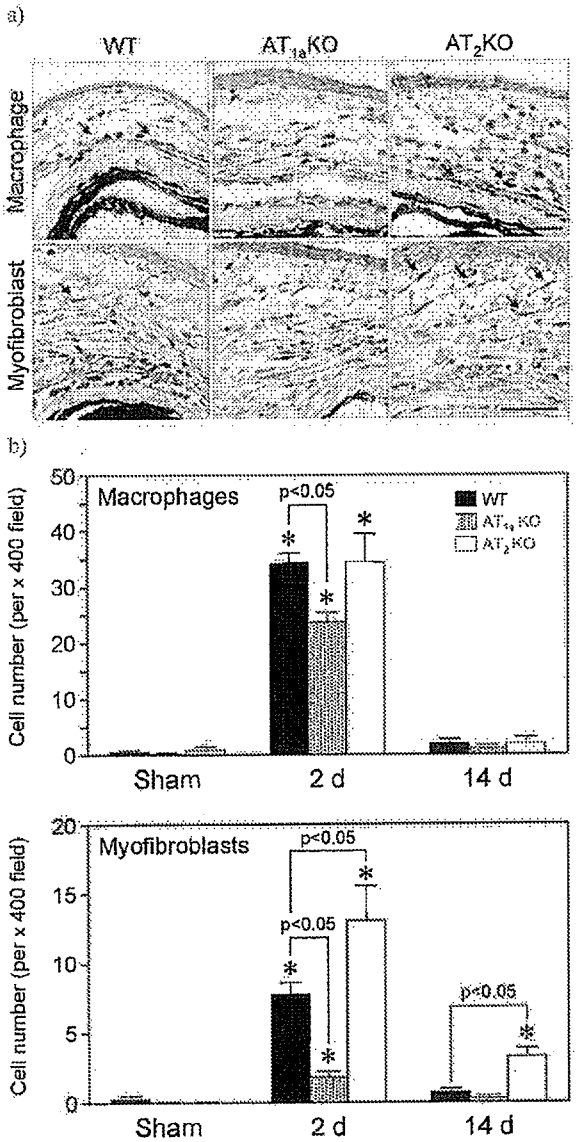

FIGURE 2 Infiltration of macrophages and myofibroblasts into subconjunctival space at 2 days after injury in AT_2KO and $AT_{1a}KO$ mice. Subconjunctival injury was induced and cross sections of eye samples were prepared as described in Figure 1. (a) Immunostaining of macrophages and myofibroblasts in subconjunctival tissue with anti-F4/80 antibody and anti-α-smooth muscle (α-SM) actin antibody, respectively. Arrows show positive staining of each marker. Magnification, ×400; scale bar, 50 μm.) (b) Changes in macrophages and myofibroblasts in subconjunctival tissue. (Sham, sham operation.) Values are mean ± SEM from 4 to 6 animals. *$p < 0.05$ versus sham group.

Collagen Deposition in Subconjunctival Space After Blunt Dissection

Subconjunctival injury induced an increase in collagen deposition during the wound-healing process. As shown in Figure 4, collagen deposition became apparent at 14 days after operation. This increase in collagen deposition was suppressed in $AT_{1a}KO$ mice, whereas it was further enhanced in AT_2KO mice (fibrosis score was 1.6 ± 0.2, 0.6 ± 0.2, and 2.7 ± 0.3 for WT, $AT_{1a}KO$, and AT_2KO mice, respectively). Figures 5a and 5b show the

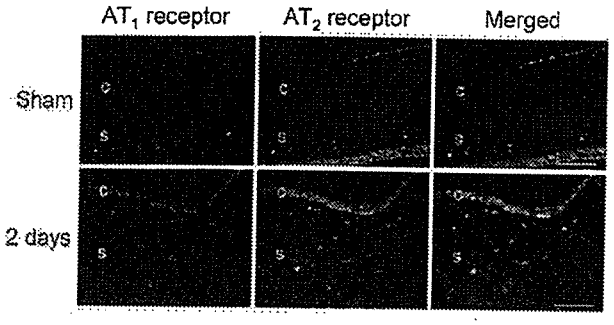

FIGURE 3 Immunofluorescence staining of AT_1 and AT_2 receptors in subconjunctival space at 2 days after injury in WT mice. Subconjunctival injury was induced and cross sections of eye samples were prepared as described in Figure 1. AT_1 and AT_2 receptors were stained using specific antibodies and fluorescent dye Cy3 (red) for AT_1 receptor and FITC (green) for AT_2 receptor, respectively, as described in "Materials and Methods." (C, conjunctiva; S, sclera; Sham, sham operation. Magnification, ×400, scale bar, 50 μm.)

expression of mRNA for collagen type I and type III in injured tissue after blunt dissection of the subconjunctiva. The mRNA levels of collagen type I and type III were markedly increased at 7 days after operation. The increase in collagen type III mRNA was significantly inhibited in AT_{1a}KO mice. In contrast, it was further enhanced in AT_2KO mice. Moreover, the increase in collagen type III mRNA was also enhanced in AT_2KO mice (Fig. 5b).

We also studied the expression of TIMP and MMP in injured tissue after operation (Figs. 5c–5f). Expression of TIMP was markedly increased at 12 hr after operation (Fig. 5c) and then decreased over the next 7 days. The increase in TIMP expression was significantly suppressed

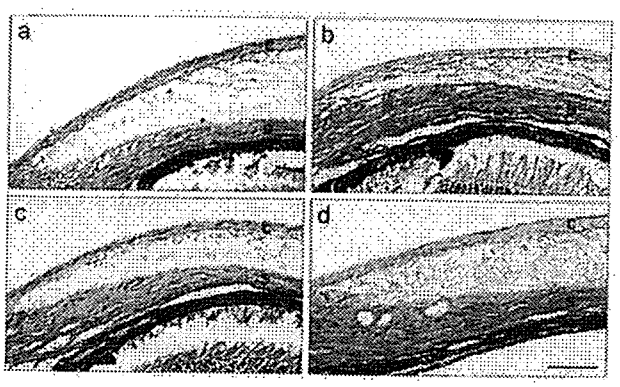

FIGURE 4 Changes in collagen deposition in subconjunctival space at 14 days after injury in sham operation (a), WT (b), AT_{1a}KO (c), and AT_2KO (d) mice. Subconjunctival injury was induced and cross sections of eye samples were prepared as described in Figure 1. Representative results of Elastica van Gieson staining of cross sections of injured eyes. n = 4 to 6. (C, conjunctiva; S, sclera. Magnification, ×400, scale bar, 50 μm.)

in AT_{1a}KO mice during first 24 hr after operation. However, it was further enhanced in AT_2KO mice, and this enhancement of TIMP expression was still observed at 7 days after operation. Among MMP subclasses, expression of MMP1 and MMP9 was not significantly altered after operation in all strains (Figs. 5e and 5f). However, expression of MMP2 was decreased during the first 24 hr after operation in all groups (Fig. 5d). MMP2 expression then recovered to the basal level in WT and AT_2KO mice, while it was significantly greater in AT_{1a}KO mice than in WT mice at 14 days after operation.

DISCUSSION

In the current study, we developed an animal model of subconjunctival injury according to the method of Reichel et al.[13] We used blunt dissection of the subconjunctiva with a spatula instead of injection of phosphate-buffered saline. Our model induced reproducible wound-healing responses, including inflammatory cell infiltration and collagen accumulation in the subconjunctival space. Using this model of subconjunctival damage, we investigated the role of Ang II receptor subtypes in the wound-healing process after ocular injury using receptor gene–deficient mice. Our results indicated that Ang II receptor stimulation is involved in the process of wound healing. It was suggested that AT_{1a} and AT_2 receptors affect wound-healing responses, such as inflammation and collagen deposition, antagonistically through regulation of MMP activity.

It is suggested that wound-healing responses include three phases; inflammation, proliferation, and remodeling.[15] These reactions are also involved in wound healing of conjunctival injury.[13] Previous reports indicated that Ang II plays an important role in the wound-healing process and tissue remodeling in various types of injury.[5–7] The receptor for Ang II has two distinct subtypes named AT_1 and AT_2 receptors.[16,17] In rodents, the AT_1 receptor is divided into two subclasses, AT_{1a} and AT_{1b}.[18] In our study, infiltration of macrophages and myofibroblasts into the subconjunctival space was also observed after subconjunctival blunt dissection. The rest of the cells in the injured tissue seemed to be neutrophils and other mononuclear cells. Such inflammatory responses were reduced in AT_{1a}KO mice, whereas the infiltration of myofibroblasts was significantly enhanced in AT_2KO mice (Fig. 2). Because the AT_{1a} receptor is a major subclass of AT_1 receptor,[4]

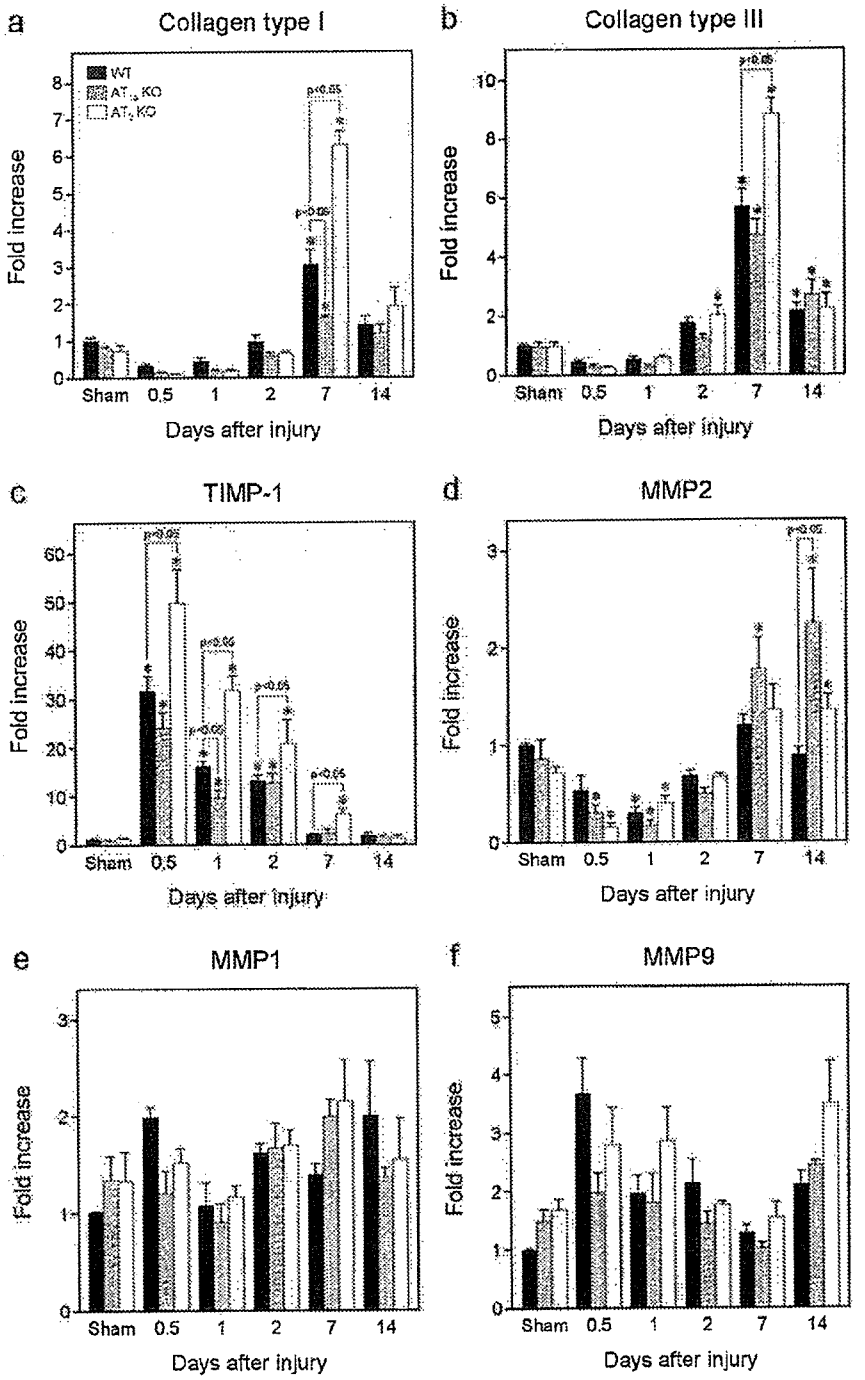

FIGURE 5 Expression of collagen type I (a), collagen type III (b), TIMP-1 (c), MMP2 (d), MMP1 (e), and MMP9 (f). Subconjunctival injury was induced and RNA samples were prepared as described in "Materials and Methods." Real-time PCR was performed as described in "Materials and Methods." mRNA levels were standardized using that of β-actin and expressed as the relative amount in WT mice of the sham group. (Sham, sham operation.) *$p < 0.05$ versus Sham. Values are mean ± SEM of 6 to 9 samples.

these results indicate that Ang II plays an important role in inflammatory responses in subconjunctival injury, and suggest that AT_1 and AT_2 receptors have antagonistic actions on regulation of the wound-healing process. Myofibroblasts as well as fibroblasts play an important role in collagen synthesis and fibrosis during wound healing.[9,19] Cleutjens et al. reported that myofibroblasts are responsible for the increase in expression of genes

encoding fibrillar type I/III procollagens.[20] It has been demonstrated that collagen production is accelerated by transforming growth factor (TGF)-β1,[21] and Ang II stimulated TGF-β1 production in fibroblasts.[19,22,23] Desmouliere et al.[24] reported that TGF-β1 induced α-SM actin expression in myofibroblasts, thereby inducing differentiation of fibroblasts into myofibroblasts. It has been reported that both TGF-β1 and β2 are activated in mouse subconjunctival tissue after surgical intervention.[25] In addition, Campbell[26] reported that an AT_1 receptor antagonist, losartan, greatly attenuated Ang II–stimulated TGF-β1 secretion in cardiac myofibroblasts. In our study, both AT_1 and AT_2 receptors were expressed in mononuclear cells infiltrating the subconjunctival space in the early phase after injury in WT mice. These results led to the hypothesis that AT_1 and AT_2 receptors regulate fibroblast activation antagonistically through TGF secretion. We have previously demonstrated that Ang II increased collagen production via the AT_1 receptor but inhibited it via the AT_2 receptor in skin fibroblasts.[11] Moreover, AT_1 receptor stimulation enhanced collagen synthesis induced by IGF-1, whereas AT_2 receptor activation inhibited it. Consistent with these results, in the current study the level of mRNA for type 1 collagen was significantly higher in AT_2KO mice but lower in AT_{1a}KO mice than in WT mice. These results suggest that the AT_1 and AT_2 receptors antagonistically regulate collagen synthesis.

It has been reported that matrix metalloproteinases (MMPs), zinc-containing Ca^{2+}-dependent endopeptidases, regulate tissue remodeling by digesting the extracellular matrix (ECM)[27] and that Ang II reduced the activity of MMP2 as well as its protein level, and these effects were inhibited by selective AT_1 receptor blockers.[28] We thus examined MMP mRNA expression in the injured subconjunctiva (Figs. 5d–5f). MMP2 mRNA was decreased during the first 24 hr after operation in all groups. The mRNA level was then recovered to the basal level in WT and AT_2KO mice but further increased in AT_{1a}KO mice. These observations suggest the possibility that AT_1 receptor stimulation causes ECM degradation, which should be clarified in future experiments.

TIMPs are known to be major endogenous inhibitors of MMPs. Four homologous TIMPs, named TIMP-1 to TIMP-4, have been identified and they similarly inhibit MMPs.[27] Especially, TIMP-1 plays an mportant role in the mouse eye.[29–31] In the current study, TIMP-1 expression was significantly lower in AT_{1a}KO mice but higher in AT_2KO mice than in WT mice in the early phase after injury (Fig. 5c). Interestingly, our group has reported that TIMP-1 expression is increased by AT_1 receptor stimulation but decreased by AT_2 receptor stimulation in mouse neonatal skin fibroblasts.[11] In accordance with our results, Chua et al.[32] reported that Ang II induced TIMP-1 production in rat endothelial cells. These results suggest that AT_1 receptor stimulation increases collagen accumulation in subconjunctival fibroblasts, at least in part, by inhibition of collagen degradation via an increase in TIMP-1 expression, whereas AT_2 receptor stimulation inhibits TIMP-1 expression, increases collagen degradation, and thereby inhibits collagen accumulation. Our group also reported that transfection of dominant negative SHP-1 (Src homology 2–containing protein-tyrosine phosphatase-1) mutant inhibited the Ang II–mediated inhibitory effect on both collagen synthesis and TIMP-1 expression in fibroblasts from AT_{1a} KO mice.[11] However, the addition of a serine/threonine phosphatase inhibitor, okadaic acid, did not affect collagen production induced by Ang II.[11] These results suggest that SHP-1 plays a pivotal role in the action of the AT_2 receptor on collagen metabolism.

In summary, we have demonstrated that the wound-healing process with collagen accumulation after ocular injury is regulated by Ang II through antagonistic actions between AT_1 and AT_2 receptors. Our results provide an insight into the pathophysiological significance of tissue Ang II in subconjunctival scarring.

ACKNOWLEDGMENTS

This work was supported by Grants-in-Aid for Scientific Research 14370559 and 15390247 from the Ministry of Education, Science, Sports and Culture of Japan, a grant from the Mitsubishi Pharma Research Foundation, and a grant from the Smoking Research Foundation.

REFERENCES

[1] Lama PJ, Fechtner RD. Antifibrotics and wound healing in glaucoma surgery. *Surv Ophthalmol.* 2003;48:314–346.
[2] Tseng SH, Chen YT, Cheng HC, et al. Impression cytology study of conjunctival epithelial phenotypes on the healing ocular surface after pterygium excision. *Cornea.* 2001;20:244–250.
[3] Tseng SC. Amniotic membrane transplantation for ocular surface reconstruction. *Biosci Rep.* 2001;21:481–489.
[4] de Gasparo M, Catt KJ, Inagami T, et al. International Union of Pharmacology. XXIII. The angiotensin II receptors. *Pharmacol Rev.* 2000;52:415–472.

[5] Rodgers KE, DeCherney AH, St Amand KM, et al. Histologic alterations in dermal repair after thermal injury effects of topical angiotensin II. *J Burn Care Rehabil.* 1997;18:381–388.
[6] Okuyama N, Roda N, Sherman R, et al. Angiotensin II improves random-flap viability in a rat model. *Ann Plast Surg.* 1999;42:313–319.
[7] Rodgers KE, Roda N, Felix JE, et al. Histological evaluation of the effects of angiotensin peptides on wound repair in diabetic mice. *Exp Dermatol.* 2003;12:784–790.
[8] Gabbiani G. The myofibroblast: a key cell for wound healing and fibrocontractive diseases. *Prog Clin Biol Res.* 1981;54:183–194.
[9] Sun Y, Weber KT. Angiotensin converting enzyme and myofibroblasts during tissue repair in the rat heart. *J Mol Cell Cardiol.* 1996;28:851–858.
[10] Nakajima M, Hutchinson HG, Fujinaga M, et al. The angiotensin II type 2 (AT2) receptor antagonizes the growth effects of the AT1 receptor: gain-of-function study using gene transfer. *Proc Natl Acad Sci USA.* 1995;92:10663–10667.
[11] Min LJ, Cui TX, Yahata Y, et al. Regulation of collagen synthesis in mouse skin fibroblasts by distinct angiotensin II receptor subtypes. *Endocrinology.* 2004;145:253–260.
[12] Ramirez M, Davidson EA, Luttenauer L, et al. The renin-angiotensin system in the rabbit eye. *J Ocul Pharmacol Ther.* 1996;12:299–312.
[13] Reichel MB, Cordeiro MF, Alexander RA, et al. New model of conjunctival scarring in the mouse eye. *Br J Ophthalmol.* 1998;82:1072–1077.
[14] Madlener M, Parks WC, Werner S. Matrix metalloproteinases (MMPs) and their physiological inhibitors (TIMPs) are differentially expressed during excisional skin wound repair. *Exp Cell Res.* 1998;242:201–210.
[15] Kirsner RS, Eaglstein WH. The wound healing process. *Dermatol Clin.* 1993;11:629–640.
[16] Whitebread S, Mele M, Kamber B, de Gasparo M. Preliminary biochemical characterization of two angiotensin II receptor subtypes. *Biochem Biophys Res Commun.* 1989;163:284–291.
[17] Chiu AT, Herblin WF, McCall DE, et al. Identification of angiotensin II receptor subtypes. *Biochem Biophys Res Commun.* 1989;165:196–203.
[18] Burson JM, Aguilera G, Gross KW, Sigmund CD. Differential expression of angiotensin receptor 1A and 1B in mouse. *Am J Physiol.* 1994;267:E260–E267.
[19] Lee AA, Dillmann WH, McCulloch AD, Villarreal FJ. Angiotensin II stimulates the autocrine production of transforming growth factor-beta 1 in adult rat cardiac fibroblasts. *J Mol Cell Cardiol.* 1995;27:2347–2357.
[20] Cleutjens JP, Verluyten MJ, Smiths JF, Daemen MJ. Collagen remodeling after myocardial infarction in the rat heart. *Am J Pathol.* 1995;147:325–338.
[21] Butt RP, Laurent GJ, Bishop JE. Collagen production and replication by cardiac fibroblasts is enhanced in response to diverse classes of growth factors. *Eur J Cell Biol.* 1995;68:330–335.
[22] Sadoshima J, Izumo S. Molecular characterization of angiotensin II-induced hypertrophy of cardiac myocytes and hyperplasia of cardiac fibroblasts. Critical role of the AT1 receptor subtype. *Circ Res.* 1993;73:413–423.
[23] Fisher SA, Absher M. Norepinephrine and ANG II stimulate secretion of TGF-beta by neonatal rat cardiac fibroblasts in vitro. *Am J Physiol.* 1995;268:C910–C917.
[24] Desmouliere A, Geinoz A, Gabbiani F, Gabbiani G. Transforming growth factor-beta 1 induces alpha-smooth muscle actin expression in granulation tissue myofibroblasts and in quiescent and growing cultured fibroblasts. *J Cell Biol.* 1993;122:103–111.
[25] Mietz H, Chevez-Barrios P, Lieberman MW. A mouse model to study the wound healing response following filtration surgery. *Graefes Arch Clin Exp Ophthalmol.* 1998;236:467–475.
[26] Campbell SE, Katwa LC. Angiotensin II stimulated expression of transforming growth factor-beta1 in cardiac fibroblasts and myofibroblasts. *J Mol Cell Cardiol.* 1997;29:1947–1958.
[27] Gomez DE, Alonso DF, Yoshiji H, Thorgeirsson UP. Tissue inhibitors of metalloproteinases: structure, regulation and biological functions. *Eur J Cell Biol.* 1997;74:111–122.
[28] Peng J, Gurantz D, Tran V, et al. Tumor necrosis factor-alpha-induced AT1 receptor upregulation enhances angiotensin II-mediated cardiac fibroblast responses that favor fibrosis. *Circ Res.* 2002;91:1119–1126.
[29] Yang YN, Bauer D, Wasmuth S, et al. Matrix metalloproteinases (MMP-2 and 9) and tissue inhibitors of matrix metalloproteinases (TIMP-1 and 2) during the course of experimental necrotizing herpetic keratitis. *Exp Eye Res.* 2003;77:227–237.
[30] Kernacki KA, Barrett R, Hazlett LD. Evidence for TIMP-1 protection against P. aeruginosa-induced corneal ulceration and perforation. *Invest Ophthalmol Vis Sci.* 1999;40:3168–3176.
[31] Majka S, McGuire P, Colombo S, Das A. The balance between proteinases and inhibitors in a murine model of proliferative retinopathy. *Invest Ophthalmol Vis Sci.* 2001;42:210–215.
[32] Chua CC, Hamdy RC, Chua BH. Angiotensin II induces TIMP-1 production in rat heart endothelial cells. *Biochim Biophys Acta.* 1996;1311:175–180.

Marx Line: Fluorescein Staining Line on the Inner Lid as Indicator of Meibomian Gland Function

MASAHIKO YAMAGUCHI, MD, MIKI KUTSUNA, MD, PHD, TOSHIHIKO UNO, MD, PHD, XIAODONG ZHENG, MD, PHD, TOSHIO KODAMA, MD, PHD, AND YUICHI OHASHI, MD, PHD

• PURPOSE: To determine whether the location of a fluorescein-stained line, the Marx line (ML), which runs along the inner eyelid, is correlated with meibomian gland function.

• DESIGN: Prospective observational case series.

• METHODS: After applying fluorescein dye solution to the eye, the ML score was calculated for the outer, middle, and inner thirds of the lower eyelid margin. ML scoring was as follows: 0, entirely on the conjunctival side of the meibomian orifices (MOs); 1, part of the ML touches the MOs; 2, ML runs through all of the MOs; and 3, ML runs on the eyelid-margin side of the MOs. Correlations were calculated between the total ML score and age for 251 randomly recruited subjects without acute ocular surface diseases, and between age and the ML score for the three regions of the lower eyelid. Correlations between the regional ML score and the meibographic score, and the meibomian gland secretion score were also determined. The total ML scores of 15 subjects without meibomian gland dysfunction (MGD) were compared with 15 age-matched patients with MGD.

• RESULTS: The three regions of the lower eyelid had significantly different ML scores. Strong correlations were found between the ML score and age, the meibographic score, and the meibomian gland secretion score. The total ML score of MGD group was significantly higher than that of the non-MGD group.

• CONCLUSIONS: The strong correlation between the ML score and the meibomian gland scores indicates that the ML score can be used as a simple and rapid screening score for meibomian gland function. (Am J Ophthalmol 2006;141:669–675. © 2006 by Elsevier Inc. All rights reserved.)

Accepted for publication Nov 8, 2005.

From the Department of Ophthalmology, University of Ehime School of Medicine, Ehime, Japan.

Inquiries to Masahiko Yamaguchi, MD, Shitsukawa, Toon City, Ehime, 791-0295 Japan; e-mail: masahiko@m.ehime-u.ac.jp

LIPIDS SECRETED FROM THE MEIBOMIAN GLANDS spread over the ocular surface by blinking and form the outer layer of the tear film to suppress evaporation.[1] These lipids also form a hydrophobic barrier at the eyelid margin that prevents the loss of tear fluid.[2] Because these two mechanisms are important for maintaining the stability of tear film, evaluation of meibomian gland function is essential when investigating the cause or treating dry eye patients.

There is a wide range of clinical examination, from simple and fast to comprehensive and time-consuming, designated to evaluate meibomian gland function. These include routine slit-lamp observations of the meibomian orifices (MOs), examination of meibomian gland sebum,[3] meibography that assesses the structure of the glands by transillumination,[4–6] meibometry that measures lipid secretion of the glands,[7,8] and analysis of meibomian gland lipids by thin-layer chromatography.[9,10] Although these methods are all valuable, a simpler test that could rapidly and accurately screen meibomian gland function is still needed for routine clinical practice.

When a fluorescent dye solution is applied to the eyelid margin, a clear line, called the Marx line (ML),[11] is recognizable, running along the inner eyelid. In normal eyes, this line is located on the conjunctival side of the MOs; however, depending on the case, the ML may be totally or partially located on the cutaneous side of the MOs.

We have hypothesized that changes in the location of the ML might be correlated with meibomian gland function. To test this hypothesis, we have determined the correlations between the ML scores and the results of more conventional tests of meibomian gland function. We also investigated the effects of aging and regional changes in the ML scores in subjects with meibomian gland dysfunction (MGD).

METHODS

THE PURPOSE OF THIS STUDY AND THE PROCEDURES TO BE used were presented to all of the subjects and patients, and

0002-9394/06/$32.00
doi:10.1016/j.ajo.2005.11.004

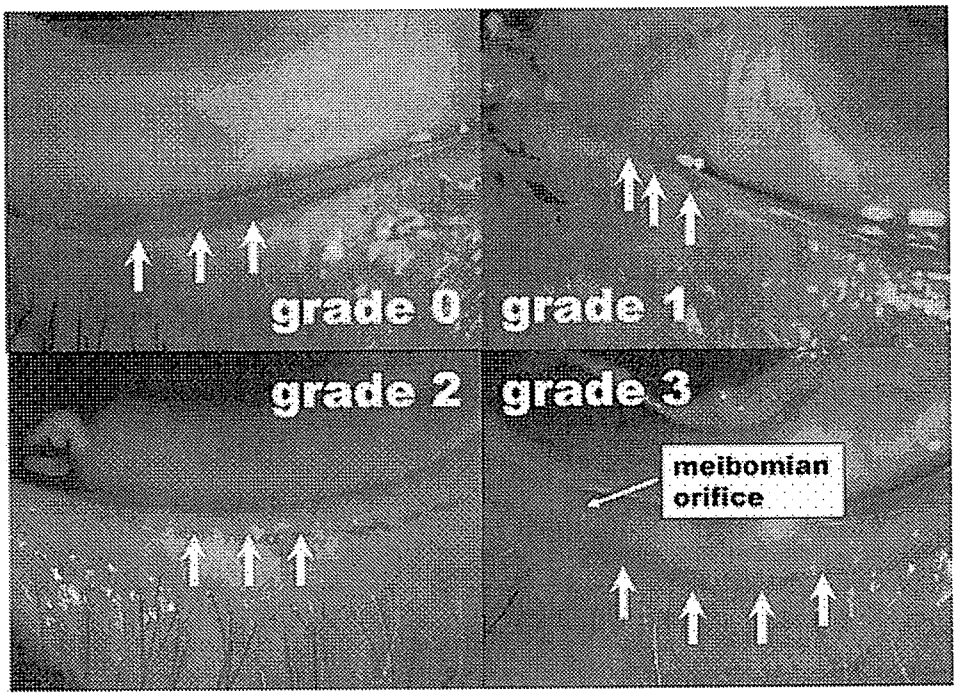

FIGURE 1. Marx line (ML) (arrows) scores: 0, fluorescein staining line running entirely along the conjunctival side of the meibomian orifices (MOs); 1, parts of the ML touching the MOs; 2, ML running through the MOs; and 3, ML running along the eyelid margin side of the MOs.

signed informed consent was obtained from each individual. The procedures used in this study conformed to the tenets of the Declaration of Helsinki.

A total of 251 subjects (105 men and 146 women, ages 59.8 ± 20.3 years [mean ± SD]) were randomly recruited from the patients who were treated at the Department of Ophthalmology of Ehime University Hospital, Ehime, Japan. None of these subjects had acute ocular surface disorders, trauma, infections, or immune diseases, such as Stevens-Johnson syndrome or ocular cicatricial pemphigoid.

The correlation between the total ML score (see below) and age was determined for the 251 subjects. In addition, among the 251 subjects, a panel of randomly selected 65 subjects (30 men and 35 women, ages 52.0 ± 23.3 years) was analyzed to determine whether a significant correlation existed between the ML score in the upper and lower eyelids. A panel of randomly selected 116 subjects (51 men and 65 women, ages 56.7 ± 17.0 years) was studied to compare the ML scores to the scores of the meibography, and another panel of 126 subjects (60 men and 66 women, ages 44.3 ± 20.2 years) was studied to compare the ML scores to the scores of the meibomian gland secretion.

To demonstrate the ML, 2 μl of fluorescein 1% solution, lissamine green B 1% solution, or rose bengal 1% solution was instilled separately into the lower fornix in 10 subjects, and after the patient blinked a few times, a stained line was observed by slit-lamp biomicroscopy along the lower eyelid. The fluorescein 1% solution was prepared by diluting fluorescein 10% solution (Fluorescite; Alcon Lab Inc, Fort Worth, Texas, USA) in saline; the lissamine green B 1% solution was prepared by dissolving lissamine green B bulk powder (Sigma Chemical Co, St Louis, Missouri, USA) in saline; and the rose bengal 1% solution was prepared by dissolving rose bengal bulk powder (Wako) in a mixture of ethyl paraoxybenzoine and propyl paraoxybenzoine. All of the solutions were sterilized by filtration through a 0.22-μm Millipore filter. There were no clinically significant adverse reactions caused by any of the solutions.

After fluorescein staining, the lower lid was examined by slit-lamp biomicroscopy, and a score was assigned according to the following criteria: 0, ML runs entirely along the conjunctival side of the MOs: 1, parts of the ML touch the MOs; 2, the ML runs through the MOs; and 3, the ML runs along the eyelid-margin side of the MOs (Figure 1).

The lower eyelid was further divided into three portions; the outer third, middle third, and inner third (Figure 2). The sum of the ML scores for the three portions of the lower lid was defined as the total score of each eye; the maximum possible ML score was 9. The mean total score was obtained by averaging ML scores of the lower eyelids of both eyes.

To estimate the accuracy of this scoring system, 20 representative photographs of the ML were individually presented to five ophthalmologists at our institution in a masked fashion, and the ML for the middle third of the lower lid was scored. As expected, the ML score for the 20 images was found to be reasonably consistent among the five ophthalmologists.